Ethanol dehydration with aerosol-made mesoporous aluminosilicates featuring dispersed active sites

Lucie Leonova[a], Giovanni Pampararo[b], Vit Vykoukal[c], Lucie Simonikova[a], François Devred[b], Pierre Eloy[b], Ales Styskalik*[a], Damien P. Debecker*[b]

[a]Masaryk University, Department of Chemistry, Kotlarska 2, CZ-61137 Brno, Czech Republic

[b]Institute of Condensed Matter and Nanoscience (IMCN), UCLouvain, Place Louis Pasteur 1, 1348 Louvain-La-Neuve, Belgium

[c]Thermo Fisher Scientific, 627 00, Brno, Czech Republic

*Corresponding author (damien.debecker@uclouvain.be, styskalik@chemi.muni.cz).

1 Abstract

Amorphous aluminosilicates are known for their excellent performance in (bio)ethanol dehydration for ethylene production. Several studies showed that the homogeneous dispersion of Al in amorphous aluminosilicates is the key to obtain active and stable catalysts. However, ensuring a high dispersion of Al in the aluminosilicate matrix remains a complicated task. Here, the aerosol-assisted sol-gel (AASG) process is presented as a facile one-step and continuous production method towards highly homogeneous aluminosilicates. We systematically examine the effect of the aluminum loading (1–9 wt.% Al) in silica matrix incorporated via AASG technique on the catalytic activity during ethanol dehydration. Aluminum dispersion, chemical structure, textural properties, and acidic behavior were investigated by STEM-EDS, MAS NMR, XPS, nitrogen porosimetry, and infrared spectroscopy combined with pyridine adsorption. Aluminum content is shown to influence textural properties and acidity, and therefore strongly modify catalytic activity. The most active AASG-prepared aluminosilicate catalysts exhibited higher activity and on-stream stability if compared to commercial silica-alumina. It reached a similar performance to other amorphous aluminosilicates with highly homogeneous Al dispersion prepared via peculiar protocols.

2 Introduction

Ethylene is nowadays one of the major bulk chemicals in petrochemical industry. Applications cover the fabrication of other important products including polyethylene, ethylene oxide, and styrene. The worldwide ethylene production capacity reached 225.5 million metric tons in 2022.[1] Consequently, a suitable industrial process including cost-effectiveness, environmental and ecological demands should be applied. Ethylene is mainly being produced via the energetically demanding steam cracking of hydrocarbons (typically operating at >800 °C),[2] or the catalytic cracking (550–650 °C)[3] or oxidative dehydrogenation of ethane (ODHE, 300–800 °C).[4] To evade such highly energetical processes, ethanol dehydration could replace current methods and be more environmentally friendly. In particular,

bioethanol can be produced at large scale made from renewable bio-based streams;[5] in this case, low carbon footprint is produced.[6] Due to the energy barriers in ethanol dehydration, widely used alumina requires elevated activation temperatures (375 °C),[7] approaching the energy requirements of ODHE.[8] Therefore, more active catalysts are being investigated to allow operating ethanol dehydration at moderate temperature. Heterogeneous catalysts based on vermiculites,[9] silicoaluminophosphates,[10,11] alumina,[9,12–14] MOFs,[15,16] resins,[17–19] heteropolyacids,[20–22] mixed metal oxides,[23–25] zeolites,[26–30] and aluminosilicates have been explored recently in alcohol dehydration.[31–38]Some of the preparation methods and catalytic performance during ethanol dehydration are summarized in Table 1.

.

The marked acidic character of aluminosilicates confers their high dehydration ability. For example, macro-mesocellular aluminosilicate monolithic foams prepared by alkaline sol-gel process based on High Internal Phase Emulsion exhibited higher amount of stronger acid sites than commercial aluminosilicate.[38] Their acidity compared to that of commercial silica-alumina made them more active in ethanol dehydration. In typical crystalline acidic zeolites (e.g. H-ZSM-5, MOR), acid sites with excessive strength can cause coke formation and rapid catalyst deactivation.[31,33,39–41] Previously studied, aluminosilicates prepared by non-hydrolytic sol-gel (NHSG) demonstrated to be an alternative to zeolites and co-precipitated silica-alumina catalyst. A catalyst prepared by NHSG (acetamide elimination route) provided high catalytic activity without extensive coking compared to zeolites.[33] The outstanding long-term stability was ascribed to the intermediate acid sites strength: while zeolites possessed strong acid sites, NHSG prepared aluminosilicates exhibited medium acid strength. The success of NHSG preparation, however, is tempered by the complicated protocol (glovebox, dehydrated organic solvents).

Table 1: Overview of catalysts applied to ethanol dehydration

Material	Preparation method	Catalytic conditions	X_{EtOH} (%)	$S_{ethylene}$ (%)	Stability[a]	ref.
Amorphous aluminosilicate (SiAl(HIPE))	Sol–gel with an emulsion-based templating	400 °C, 99.7 wt.% bioethanol, 23.8 h^{-1} WHSV	97	95	not studied	[38]
HZSM-5 zeolite	Commercial sample	240 °C, 1 atm, absolute ethanol, 1.1 h^{-1} WHSV	100	100	conversion drop by 20 % after 15 h[b]	[33]
Amorphous aluminosilicate (16Si-1Al-Ac-T)	Non-hydrolytic sol-gel	240 °C, 1 atm, absolute ethanol, 1.1 h^{-1} WHSV	86	55	stable conversion for 15 h[c]	[33]
ZSM-5 zeolite (Z11)	Hydrothermal crystallization	240 °C, 100 $mmol_{EtOH}$ h^{-1} g_{cat}^{-1}	100	100	conversion drop by 7.4 % after 60 h	[27]
ITQ zeolite (ITQ-6_30)	Delaminated form of ferrierite	225 °C, 100 mg catalyst, 3.3 vol%. EtOH, 20 mL min^{-1} He total flow rate	100	100	not studied	[42]
Montmorillonite intercalated with mixed metal oxides (PCH-Al(TIE1))	Intercalation, templated ion exchange	250 °C, 1 atm, 100 g catalyst, 5.7 vol%. EtOH, 20 mL min^{-1} He total flow rate	~60	~40	conversion drop by 3 % after 8 h	[43]
Zeolite β (β-MW-Nano)	Microwave synthesis	260 °C, 4 MPa, 1.78 h^{-1} WHSV	47.46	~100	conversion drop by ~8 % after 10 h[d]	[26]

MFI zeolite	Sonochemical synthesis of MFI type zeolite	250 °C, 2.0 h^{-1} WHSV	84	66	not studied	[44]
ZSM-5 grafted with trifluoromethanesulfonic acid (H-ZSM-5/TFA)	Grafting	200 °C, 10 wt.% EtOH in water, 1.1 h^{-1} WHSV	97.3	99.9	stable for hundreds of h	[45]
γ-Al_2O_3 (A)	Commercial sample	250 °C, 1 atm, 96 % EtOH, 1.43 h^{-1} WHSV	78.6	20.2	not studied	[12]
Amorphous silica alumina (SA87)	Commercial sample	250 °C, 1 atm, 96 % EtOH, 1.43 h^{-1} WHSV	67.5	35.1	not studied	[12]
MFI zeolite (H-MFI (280))	Commercial sample CBV 28014	250 °C, 1 atm, 96 % EtOH, 1.43 h^{-1} WHSV	~80	~30	not studied	[31]
H-FER zeolite (H-FER)	Commercial sample CP 914C	300 °C, 1 atm, 96 % EtOH, 1.43 h^{-1} WHSV	100	99.9	stable for 405 min	[31]
Hierarchical H-ZSM-5 zeolite (Hie-HZSM-5-F2.50]	Hydrothermal synthesis	300 °C, 99.5% EtOH, 0.72 h^{-1} WHSV	99.8	~95	stable for 48 h	[28]

[a]some of the catalyst deactivation were studied at full conversion, thus the catalyst could be more active[46]

[b]240 °C, 1 atm, absolute ethanol, 2.34 h^{-1} WHSV[33]

[c]275 °C, 1 atm, absolute ethanol, 17.5 h^{-1} WHSV[33]

[d]340 °C, 6.5 MPa, WHSV 1.78 h^{-1}

NHSG[47,48] shares some benefits of mixed oxides preparation with the aerosol-assisted sol-gel technique.[49] Both methods enable the synthesis of amorphous, porous materials with controllable composition and highly homogeneous structures at the atomic scale.[50,51] This homogeneity results from the method's protocol.[52] Briefly, in the aerosol-assisted sol-gel method, hydrolysis forms a colloidal suspension of small particles prior to their polycondensation, gelation, aging, and drying. The four latter steps are completed within seconds during the processing of the aerosol droplets, and therefore the system tends to reach a metastable state resulting in materials with statistically distributed composition.[53] Moreover, the aerosol-assisted sol-gel process is easily scalable to industrial levels and does not produce solid waste. It also allows synthesis from readily available, inexpensive precursors, enhancing the technique's versatility and efficiency.

Aerosol-assisted sol-gel preparation of aluminosilicates has been reported in a handful of scholarly publications. The sol-gel pre-hydrolysis can be performed in either acidic (HCl[54]) or basic (tetrapropylammonium hydroxide[55,56]) media and with various templating agents (F127[55,56], hexadecyltrimethylammonium bromide[54]). Usually, tetraethyl orthosilicate (TEOS) serves as precursor while aluminum precursor differs (e.g. aluminum tri-*sec*-butoxide[55,56], aluminum isopropoxide or aluminum chloride[54]). On the one hand, using aluminum isopropoxide in both traditional hydrolytic and aerosol-assisted sol-gel methods resulted in a higher aluminum incorporation compared to incorporated silicon as the rate of acid hydrolysis of aluminum precursor is faster. It led to the higher Al/Si ratios than nominal.[54,57] Therefore, the real ratio is challenging to control in the case of using aluminum isopropoxide. On the other hand, application of aqueous aluminum chloride in aerosol-assisted sol-gel provided a good Al dispersion as inferred from an agreement between Al/Si ratio in bulk and surface layer.[54] The aerosol-assisted sol-gel method is highly adjustable in terms of operating conditions, and this translates into tunable materials properties such as pore size and acidity.[56] This feature makes AASG-made aluminosilicates promising candidates for various catalytic applications. Their application even extends beyond this study when aluminosilicates are doped with other metals using the aerosol strategy (e.g. in Mo- and W-catalyzed olefin metathesis[58,59]).

In this paper, we have synthetized aluminosilicate catalysts starting from TEOS and aluminum nitrate nonahydrate by means of the aerosol-assisted sol-gel technique. Aluminum nitrate nonahydrate offers a promising alternative precursor for aluminosilicates synthesis due to its cost-effectiveness, hydrophilic character that facilitates controlled hydrolysis for homogeneous products, lower toxicity, and ease of storage and handling during AASG process. This previously unused starting chemical during AASG synthesis could positively contribute to the synthesis process, making it safer and more efficient compared to traditional precursors such as alkoxides. Additionally, to the best of our knowledge, AASG-prepared aluminosilicate catalysts have not yet been applied to ethanol dehydration, and they could significantly impact the development of previously prepared aluminosilicate catalysts that have been characterized by low activity, rapid deactivation, or challenging scale-up.

We discuss the impact of the aluminum content in the siliceous matrix on textural properties, aluminum dispersion, and acidity. From this detailed characterization we elucidate the catalytic behavior of these porous aluminosilicates in ethanol dehydration. Notably, the catalytic performance of low-loaded aluminosilicates was higher than that of commercial silica-alumina. This research forms the foundation for further studies, highlighting the importance of well-characterized aluminosilicates prepared by industrially scalable technique. The omnipresent application of aluminosilicate-based materials underscore the

importance of herein synthesized samples for extended applications in heterogeneous catalysis and related fields (i.e., adsorption, separation processes, gas storage).[60–64]

3 Experimental section

Instrumentation, spectroscopic data, and data obtained during catalytic experiments can be found in Supplementary Materials.

3.1 Catalysts synthesis

A series of aluminosilicates with varying Al/Si ratio was prepared by aerosol-assisted sol-gel technique (Figure S1) according to the following recipe (Table 2). Typically, TEOS (TCI Chemicals, >97.0 %) was dissolved in diluted hydrochloric acid (20 g, 0.01 mol L^{-1}, Roth, 37 wt.%). In the second Erlenmeyer flask, amphiphilic block copolymer Pluronic F-127 (3.88 g, Sigma Aldrich, $\simeq$ 12600 g mol^{-1}) was dissolved in absolute ethanol (45 g, VWR, >99.8 v/v%) and distilled water (8 g). TEOS, diluted hydrochloric acid, Pluronic F-127, distilled water, and absolute ethanol were weighted using balance VWR® Science Education Precision Balances, while aluminum nitrate nonahydrate was weighted using analytical balances (A&D Company, Limited) with precision of 0.1 mg. Precise amounts of chemicals used for each sample are summarized in Table S1. Both mixtures were stirred overnight to obtain homogeneous solutions. Then, the former solution was added to the solution of Pluronic F-127 and after a minute of stirring, corresponding amount of aluminum nitrate nonahydrate (Table 2, ACS reagent, ≥98%) was directly added to the solution. Prior to atomization in a TSI aerosol generator (model 9306, 30 psi of air), the solution was stirred for 30 min. The aerosol droplets are processed in a horizontal tubular furnace set at 450 °C. Dried powder was collected on a cellulose nitrate filter. To remove the template, recovered powder was calcined under static air: (i) heating to 350 °C (heating ramp 1 °C min^{-1}) and 3 hours of dwelling (ii) heating to 550 °C (heating ramp 1 °C min^{-1}) and 3 hours of dwelling. Samples were labeled as SiAlX where X corresponds to the nominal aluminum weight percent (Table 2). For comparison pure silica was prepared in the same way without addition of any aluminum precursor. Benchmark sample (commercial silica-alumina support grade 135, SACS, with ca. 6.5 nominal Al wt.% was obtained from Merck and used as received. Washing was applied as an alternative template removal method. In such case, the sample (0.602 g) was heated in EtOH (30 mL) at 70 °C for 40 hours followed by filtration over Büchner funnel (0.55 mm filtration paper). The washed powder was recovered after drying at 110 °C.

Table 2: Synthesis parameters of aluminosilicates prepared by aerosol-assisted sol-gel method

sample	c(Al) (wt.%)	m(TEOS) (g)	n(Si) (mol)	m($Al(NO_3)_3 \cdot 9H_2O$) (g)	n_{Al} (mmol)	n_{Al}/n_{Si} nominal	n_{Al}/n_{Si} ICP-OES
SiO2	0	12.033	57.76	0	0	0	0
SiAl1	1	12.007	57.63	0.4869	1.3	0.022	0.023
SiAl3	3	12.022	57.71	1.4893	4.0	0.069	0.071
SiAl5	5	12.007	57.63	2.5334	6.8	0.117	0.122
SiAl7	7	12.026	57.73	3.6251	9.7	0.168	0.175
SiAl9	9	12.024	57.72	4.7591	12.7	0.220	0.227

3.2 Adsorption of trimethyl phosphine oxide (TMPO)

The adsorption of trimethyl phosphine oxide (TMPO) was used for determination of acid sites in aluminosilicates and deeper elucidation of aluminum distribution over silicate matrix.[33]

Selected samples (SiAl1, SiAl3, SiAl9, and SACS) were degassed at 350 °C under a vacuum (~10^{-3} Torr) overnight. TMPO (abcr, 95 %) dissolved in dry dichloromethane (0.2525; 0.2641 or 0.4113 wt.%) was directly added to the sample under dry nitrogen atmosphere to ensure the ratio $n_{TMPO} : n_{Al}$ = 1.2 for SiAl1 and $n_{TMPO} : n_{Al}$ = 1.0 for SiAl3, SiAl9, and SACS. The mixture was stirred overnight at room temperature, and the volatiles were removed via distillation at 150 °C under dynamic vacuum overnight. Solid products denoted as SiAl1+TMPO, SiAl3+TMPO, SiAl9+TMPO, and SACS+TMPO were analyzed by magic angle spinning nuclear magnetic resonance spectroscopy (MAS NMR).

3.3 Ethanol dehydration:

The air-exposed catalysts (0.189 g, sieved 0.2–0.4 mm particle size range; around 15–16 wt.% of moisture determined by ICP-OES) were loaded in a fixed bed vertical stainless-steel reactor (ID = 60 mm). The void space of the reactor was filled with glass beads (0.5−1 mm) to achieve a homogeneous distribution of the reaction mixture. The catalytic tests were carried out at atmospheric pressure, WHSV = 1.1 h^{-1}. Catalytic testing was carried out by injecting 0.208 g h^{-1} of absolute ethanol utilizing NE-300 syringe pump. Ethanol with 5 mol% of pentane (internal standard) was fed in a 40 mL min^{-1} flow of N_2 (4.05 mol% of absolute ethanol (VWR, > 99.8 %) in the mixture of N_2, absolute ethanol, and pentane (Roth, >99 %)). One dose of catalyst was subjected to sequential temperature variations from 170 to 310 °C by steps of 35 °C during a single catalytic run. Effluent gases (4 injections at each temperature within 60 min) were analyzed in line on a Varian 3800 gas chromatograph equipped with a flame ionization detector (FID) and a Restek Rt-U-BOND (30 m long, internal diameter 0.32 mm, film thickness 10 µm). The oven temperature was programmed as follows: initially set to 110 °C for 6 minutes, followed by a ramping rate of 10 °C min^{-1} to reach 150 °C and a dwell time of 4 minutes. 1 minute is required to cool down.

Catalyst stability over fresh catalysts (SiAl1, SiAl3, SACS) was performed at 240 °C for 48 h keeping the same conditions. For SiAl3, to account for the relatively high activity, the catalyst amount was lowered to 0.147 g (sieved, 0.2–0.4 mm particle size range) instead of 0.189 g to ensure reliable comparison at iso-conversion (i.e., WHSV reached 1.4 h^{-1} in this experiment).

An additional experiment was conducted to elucidate the catalyst regeneration process. Fresh SiAl3 (0.147 g, particle size 0.2–0.4 mm) was subjected to 48 hours on stream under the same conditions as the stability test (WHSW = 1.4 h^{-1}). After 48 hours, the feed of the reaction mixture was stopped, and the catalyst was purged with nitrogen for 20 min to remove residual ethanol vapors. Subsequently, the furnace temperature was increased up to 550 °C (with heating ramp 1 °C min^{-1}), and additionally an oxygen flow (10 NmL min^{-1}) was applied. After a temperature reached 550 °C, the furnace temperature was lowered to 240 °C, the oxygen flow was stopped, and the reaction mixture was re-introduced.

Ethanol conversion (X_{EtOH}) was calculated as:

$$X_{EtOH} = 100 \cdot (n_{EtOH,in} - n_{EtOH,out})/n_{EtOH,in}$$

Selectivity to product i (S_i) was calculated as:

$S_i = 100 \cdot n/(v_i \cdot n_{EtOH,in} - n_{EtOH,out})$

Yields (Y_i) were calculated as:

$Y_i = S_i \cdot X_{EtOH}/100$

where n is a molar flow of compound and v_i is the ratio of stoichiometric reaction coefficients.

4 Results and discussion

4.1 Synthesis and textural properties

Aerosol-assisted sol-gel synthesis was applied for the preparation of aluminosilicates with various aluminum content. Addition of aluminum precursor - nonahydrate aluminum nitrate - before spray-drying allows an immediate incorporation of metal into a silica structure like in the case of tin[65] or gallium[66] silicates. We have chosen mildly acidic conditions for the prehydrolysis of precursors, included pore-generating agent Pluronic F-127, and varied aluminum content from 1 wt.% to 9 wt.% keeping other synthetic parameters and process conditions constant.

The AASG process usually produces spherical microparticles, as a reminiscence of the spherical aerosol droplets that are processed.[54,65,67] Accordingly, spherical aluminosilicate particles with sizes in the 40 to 4000 nm range (Figure S2) were observed by scanning electron microscopy (SEM) for all aluminum loadings after calcination (Figure 1). Infrared (IR) spectroscopy (Figure 2) confirmed the presence of aluminosilicate network thanks to the typical vibration band at 1050–1038 cm^{-1} with a shoulder at 1090 cm^{-1} corresponding to the asymmetric stretching vibration of Si–O–Si/Al bonds. Both absorption bands shifted to lower frequencies with increasing aluminum content, as classically observed in the case of zeolites (though the shift is more marked in the case of zeolites, 950–1090 cm^{-1}).[68] The intensity of the absorption band at 940 cm^{-1} slightly increases as the aluminum content increases. The latter band comes from the Si–OH stretching vibration. Its increase in intensity is related to the presence of a higher amount of Si–O–Al bonds and thus more silanol (bridging) SiO(H)Al groups.[69] No significant vibrations around 3000 cm^{-1} are visible (ν C–H) meaning that organic templating agent was successfully removed during calcination.

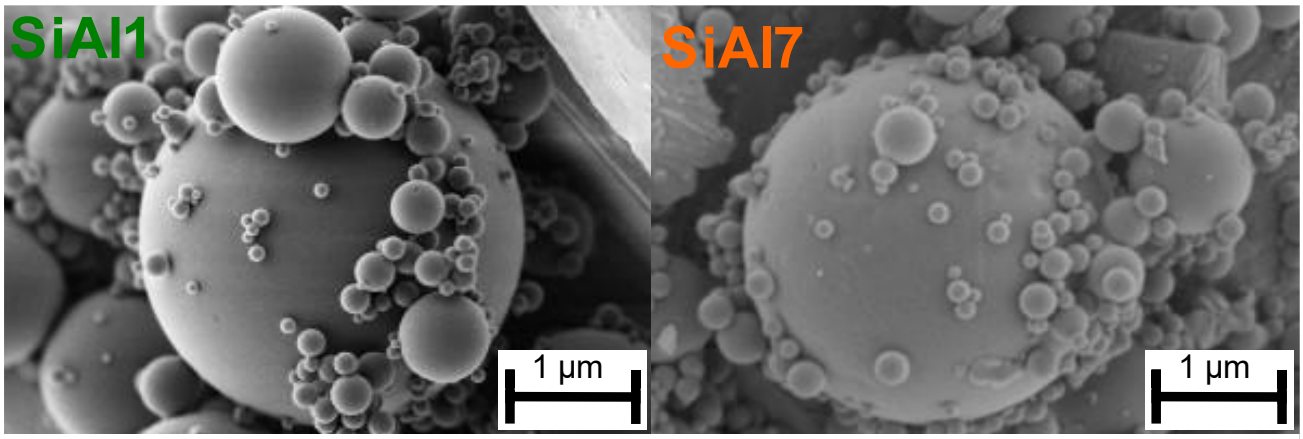

Figure 1: Scanning electron microscopy micrograph of SiAl1 (left) and SiAl7 (right)

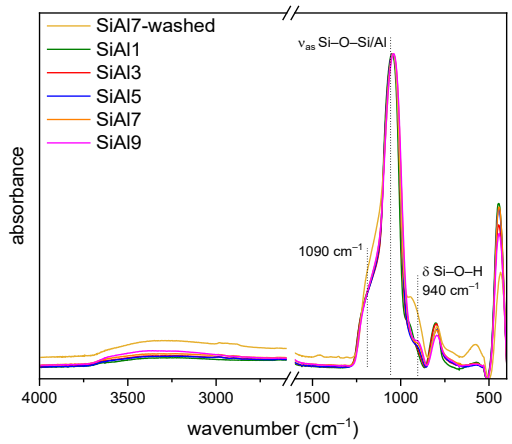

Figure 2: ATR-infrared spectra of aluminosilicates

The sample texture was investigated by nitrogen physisorption. Owing to the adopted sacrificial template, this aerosol-assisted sol-gel method is known to yield highly mesoporous materials with relatively uniform pores, which is a pivotal property of materials used in catalysis.[70] However, the isotherms of calcined samples (Figure 3) change dramatically with varying aluminum content. Samples with a lower aluminum contents (up to 5 wt.%) feature type IV isotherms with a H2 hysteresis loop (indicating the presence of open mesopores) typical for AASG prepared metallosilicates as shown elsewhere.[65,71] Samples with 7 and 9 wt.% Al show very low nitrogen uptakes indicating low porosity. Presence of mesopores in **SiAl1**, **SiAl3**, and **SiAl5** is confirmed by Barrett-Joyner-Halenda (BJH) pore size distribution (Figure 3) which is narrow and only one pore size maximum appeared. With increasing aluminum content, the most abundant pore size is shifted to lower values, from 7.3 nm for pure silica down to 4.6 nm for **SiAl3** and **SiAl5**.

While pure silica exhibited a specific surface area of 370 $m^2\ g^{-1}$ (similarly elsewhere[71]) with total pore volume reaching 0.52 $cm^3\ g^{-1}$, the addition of aluminum reduced the specific surface area and shrinked pore volume gradually down to 190 $m^2\ g^{-1}$ and 0.19 $cm^3\ g^{-1}$ for **SiAl5**, respectively. The decreasing porosity for sol-gel derived and coprecipitated silica-alumina (0–10 Al wt.%) was reported elsewhere.[72] The micropore content was influenced by the aluminum loading as well: the highest micropore content based on pore volume was observed for **SiAl1** (34 %) and decreased with Al content down to 30 % for **SiAl5**. Micropore surface area increased with increasing aluminum content. Interestingly, the pure silica stood out from these trends with only 9.3 % micropore volume and 24 % micropore surface area showing a dramatic impact of even a low Al content on textural properties.

Strikingly, the porous structure completely collapsed for aluminosilicates with higher loadings as already indicated by the isotherms shape (**SiAl7** and **SiAl9**, Table 3). Specific surface areas dropped down to 18 and 29 $m^2\ g^{-1}$ for **SiAl7** and **SiAl9** and the total pore volumes also markedly shrunk down to 0.029 and 0.046 $cm^3\ g^{-1}$, respectively). These drastic changes in textural parameters clearly point to a (partial) structural collapse of the ordered materials.[73]

Ethanol washing was applied to **SiAl7** instead of calcination to verify if the pore collapse can be avoided. Ca. 46 % of the starting mass of non-calcined **SiAl7** was removed by alcohol washing. The percentage roughly corresponds to the Pluronic F-127 amount used for the synthesis and therefore most of the organic polymer appears to be effectively washed out. TG-DSC of as-synthesized **SiAl7** confirmed similar mass loss up to 1000 °C (42.4 %, Figure S3). For the **SiAl7-washed** sample, nitrogen physisorption isotherms

resembled those of **SiAl3** and **SiAl5** (Figure 3) and the specific surface area reached 319 $m^2\ g^{-1}$ and total pore volume reached 0.32 $cm^3\ g^{-1}$. The mesopore size distribution and the micropore content were also very similar to samples **SiAl1**, **SiAl3**, and **SiAl5**. Therefore, we ascribe the pore collapse observed in **SiAl7** and **SiAl9** to the combination of higher Al loadings (possibly many strained Si–O–Al bonds) with the calcination process. The calcination process may trigger the metal migration.[58] On the one hand, X-ray diffraction analysis of calcined **SiAl9** provided only amorphous character of silica matrix and thus crystalline aluminum (or silicon) oxide phases were not formed (X-ray diffractogram shown in Figure S4). On the other hand, separation of alumina-rich and silica-rich amorphous phases in **SiAl7** and **SiAl9** cannot be excluded by X-ray analysis and therefore aluminum dispersion should be explored in more detail (see below).

In the end, our proposed protocol for preparation of porous aluminosilicate structure out of aluminum nitrate nonahydrate by aerosol-assisted sol-gel process can be considered as versatile for both low and high aluminum loadings. Al incorporation perfectly fits with nominal loadings and porous structure can be maintained.

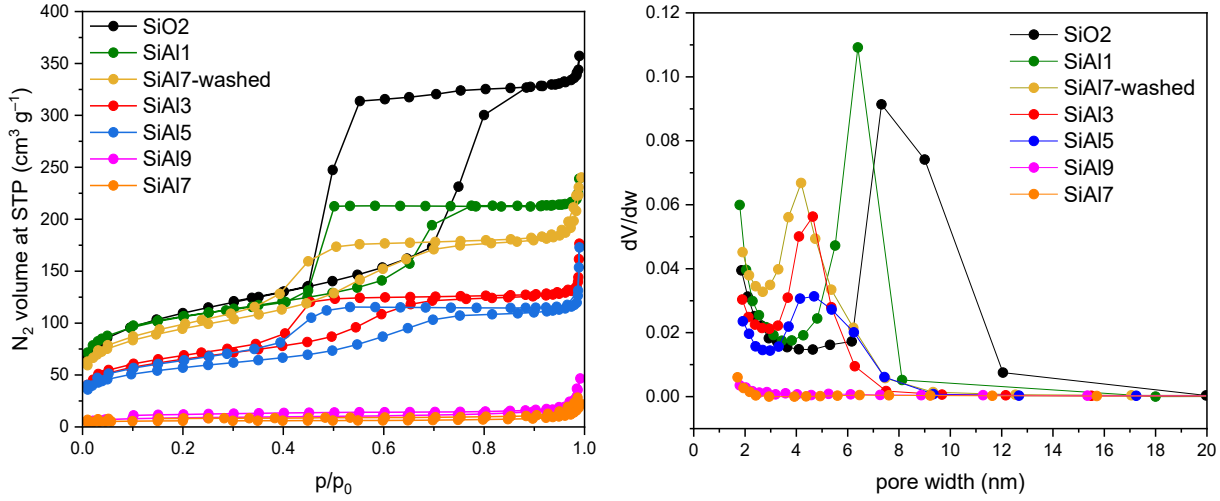

Figure 3: Adsorption desorption isotherms of aluminosilicates (left) and BJH adsorption: pore size distribution (right) of AASG prepared aluminosilicates

Table 3: Overview of porosity properties over aluminosilicates compared with pure silica

sample	Al wt.%	SA_{BET} ($m^2\ g^{-1}$)	[a]V_{total} ($cm^3\ g^{-1}$)	D (nm)	V_{micro}/V_{total} (%)	SA_{micro}/SA_{total} (%)
SiO_2	0	370	0.52	7.1	9.3	24
SiAl1	1	350	0.32	5.2	34	58
SiAl3	3	220	0.21	5.8	33	59
SiAl5	5	190	0.19	7.3	30	56
SiAl7	7	18	0.03	18	6.1	29
SiAl9	9	29	0.04	21	3.0	23
SiAl7-washed	7	319	0.32	5.5	30	58

[a]total pore volume at $p/p_0 = 0.98$

4.2 Aluminium dispersion and acidity

AASG usually provides a good metal dispersion through the silica matrix due to quick steps of sol-gel process completed within seconds (a phenomenon that has been denoted as “kinetic quenching”).[51,71] We have performed Scanning Transmission Electron Microscopy with Energy Dispersive X-ray Spectroscopy (STEM-EDS), compared aluminum content in bulk (by Inductively Coupled Plasma Atomic Emission Spectroscopy, ICP-OES) and surface layer (by X-ray photoelectron spectroscopy, XPS), and collected ^{27}Al MAS NMR spectra to elucidate aluminum dispersion over the material.

First, STEM-EDS was measured for the sake of analysis of metal distribution over two chosen aluminosilicates – **SiAl1** and **SiAl7** as representatives of one with low Al content (porosity retained) and one with high Al content (pore structure collapsed), respectively. **SiAl7-washed** was analyzed as well for comparison (Figure 4). The aluminum distribution was always homogeneous and no clusters in the form of separate alumina-rich domains were observed.

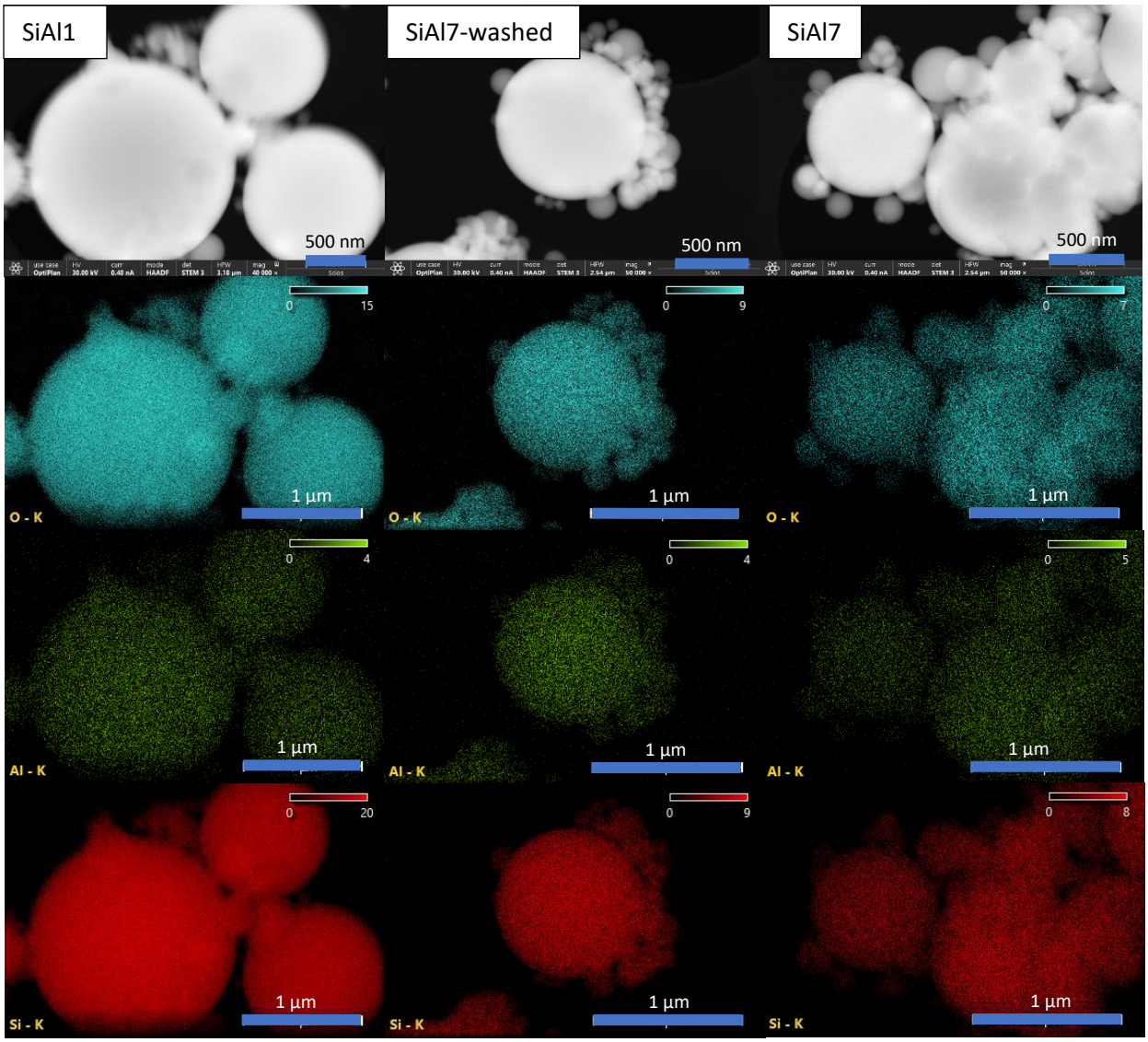

Figure 4: STEM-EDS micrographs of SiAl1, SiAl7-washed, SiAl7 (numbers below the color scale bar represents number of counts)

Second, considering the Al bulk concentration in the siliceous matrix, elemental analysis (ICP-OES) confirmed the full Al incorporation: the nominal and bulk Al/Si ratios were in excellent agreement (Table 4). The surface molar Al/Si ratio (XPS), however, was somewhat lower than the bulk ratio for all samples. Yet, the bulk and surface molar Al/Si ratios (Figure 5) followed each other relatively closely. Therefore, it may corroborate that the aluminum inserted in the silicate structure was well-dispersed.

High resolution XPS spectra of Al 2p provided further insight into aluminum speciation in silica. Data are summarized in Table S2. The Al binding energy was in the 75.0–75.6 eV range, which is clearly higher than the binding energy of Al 2p in pure Al_2O_3 (74.1 eV). This corroborates the incorporation of Al atoms in the silica matrix of aerosol-made aluminosilicates, where Al atoms are mostly bonded (via oxo bridges) to more electronegative silicon atoms.[74] In fact, Al 2p binding energy of AASG-prepared aluminosilicates

closely resembled binding energy of commercial zeolite HZSM-5 (75.2 eV, see Supplementary materials, Table S1), further confirming the insertion of Al species in the silica matrix. Finally, the carbon contribution in the form of C–(C,H), C–O, O–C–O, and O=C–O in the spectra only coming from the adventitious carbon confirmed the complete removal of the templating agent as indicated already by IR spectroscopy (Figure 2) and nitrogen physisorption (Figure 3). The $n_{C/Si}$ ratio is slightly increasing with aluminum content (Table 4) except for **SiAl7-washed** where carbon content was double (Table S2) compared to **SiAl7**. The trend of increasing adventitious carbon content with increasing aluminum concentration in alumina-silica materials was already observed elsewhere.[75]

Table 4: Elemental analysis determined by XPS and ICP-OES compared to nominal values

sample	Bulk – nominal synthesis	Bulk – ICP-OES	Surface – XPS			Surface – STEM-EDS
	n_{Al}/n_{Si}	n_{Al}/n_{Si}	n_{Al}/n_{Si}	n_O/n_{Si}*	n_C/n_{Si}	n_{Al}/n_{Si}
SiO_2	–	–	–	–	–	–
SiAl1	0.022	0.023	0.018	3.1	0.15	0.033
SiAl3	0.069	0.071	0.020	3.1	0.20	–
SiAl5	0.12	0.12	0.098	2.8	0.16	–
SiAl7	0.17	0.18	0.13	2.8	0.26	0.21
SiAl7-washed	0.17	–	0.14	2.8	0.56	0.20
SiAl9	0.22	0.23	0.19	3.4	0.29	–
SACS	~0.15	~0.13	0.16	2.9	0.28	–

*oxygen attached to carbon (CO bonds) included

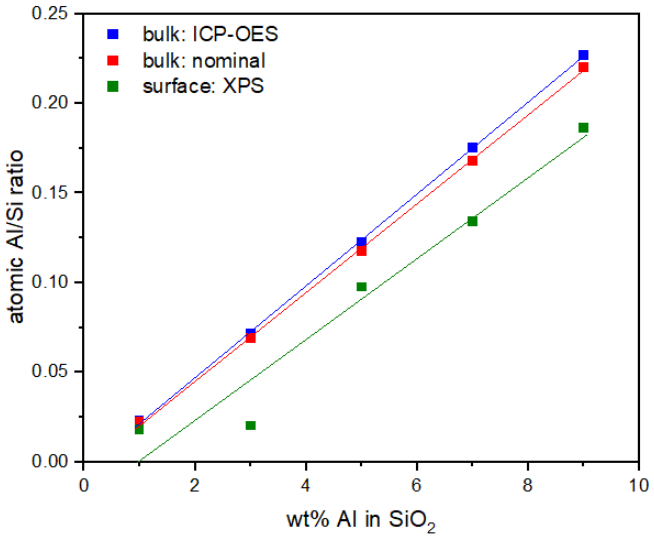

Figure 5: Atomic Al/Si ratio over nominal concentration of Al in SiO_2 determined by nominal ratio, ICP-OES, and XPS

Third, ^{29}Si cross polarization (CP) MAS NMR and ^{27}Al MAS NMR spectroscopy (Figure S5 and Figure 6A) were used to elucidate the nature of silicon and aluminum species in the silica matrix and further support

previous conclusions about aluminum dispersion. Silicon was present in the form of Q^4, Q^3, and Q^2 tetrahedra, as expected (Figure S5).[72,76] Incorporation of aluminum atoms in the silica matrix via AASGgenerated mostly tetrahedral AlO_4 sites. The presence of five-coordinated and six-coordinated aluminum species was more pronounced in the case of **SiAl7** and **SiAl9**, i.e. the samples with higher Al loadings. It appears, that calcination triggered AlO_5 and AlO_6 formation, especially in the case of high Al loadings as: (i) as-synthesized **SiAl1** exhibited visually similar fraction of different Al coordination as calcined **SiAl1** (Figure S6, left), (ii) **SiAl7-washed** possessed lower fraction of AlO_6 and AlO_5 compared to calcined **SiAl7** (Figure S6, right). Noteworthy, higher AlO_5 and AlO_6 species content was also observed at higher Al loadings (e.g. 13 wt.% Al_2O_3) in aluminosilicates presented elsewhere.[77,78]

There are several possible explanations for the pronounced AlO_6 formation in samples with higher Al loadings. First, it can result from the higher amount of coordinating water causing the transformation of well-incorporated four-coordinated Al atoms into six-coordinated ones.[79,80] Second, six-coordinated atoms can also be established due to high calcination temperatures (as discussed above) leading to Al diffusion and Al oxide oligomers formation (clustering): separate alumina phase – extraframework aluminum species are created.[60,78,81] Considering the fact, that the aerosol-assisted sol-gel technique is deemed to provide high dispersion of metals[58,59,65,70] into the materials, we aimed to verify preliminary results from STEM-EDS and XPS and confirm the formation of well-inserted aluminum atoms in the position of silicon creating tetrahedral coordination. Thus, we have investigated chosen samples, specifically **SiAl1**, **SiAl3**, **SiAl9** and SACS (for comparison), by ^{27}Al MAS NMR after sample degassing and adsorption of trimethyl phosphine oxide (TMPO; kinetic diameter = 0.55 nm)[82] (Figure 6B). Noticeably, only tetrahedrally-coordinated Al atoms with a chemical shift of 50 ppm are observed in the spectra of **SiAl1+TMPO** and **SiAl3+TMPO**. As there is not even a small indication of octahedrally-coordinated aluminum atoms, the presence of AlO_6 species (as in the Figure 6A) appears only when it is exposed to air probably via water molecules coordination (as suggested above). Thus, extraframework aluminum species are excluded in **SiAl1** and **SiAl3**. For Al highly loaded sample - **SiAl9+TMPO** – the broad signals in ^{27}Al MAS NMR spectra prevent clear identification of Al coordination. The absence of phosphorus signals in the ^{31}P MAS NMR spectra (Figure 6C) confirms that TMPO does not coordinate to Al sites, leading to asymmetric Al environments and large quadrupole splitting in ^{27}Al MAS NMR spectrum (Figure 6B). Similar behavior has already been reported earlier.[83,84] For SACS+TMPO, besides the mostly abundant tetrahedrally-coordinated aluminum atoms, a signal at 38 ppm and a broad baseline feature hiding possible signals of penta/hexacoordinated Al atoms appeared. A chemical shift of 34 ppm was linked to extraframework species in non-hydrated zeolite Y,[85] and prior studies on metal dispersion of SACS further support the presence of alumina-rich domains.[33]

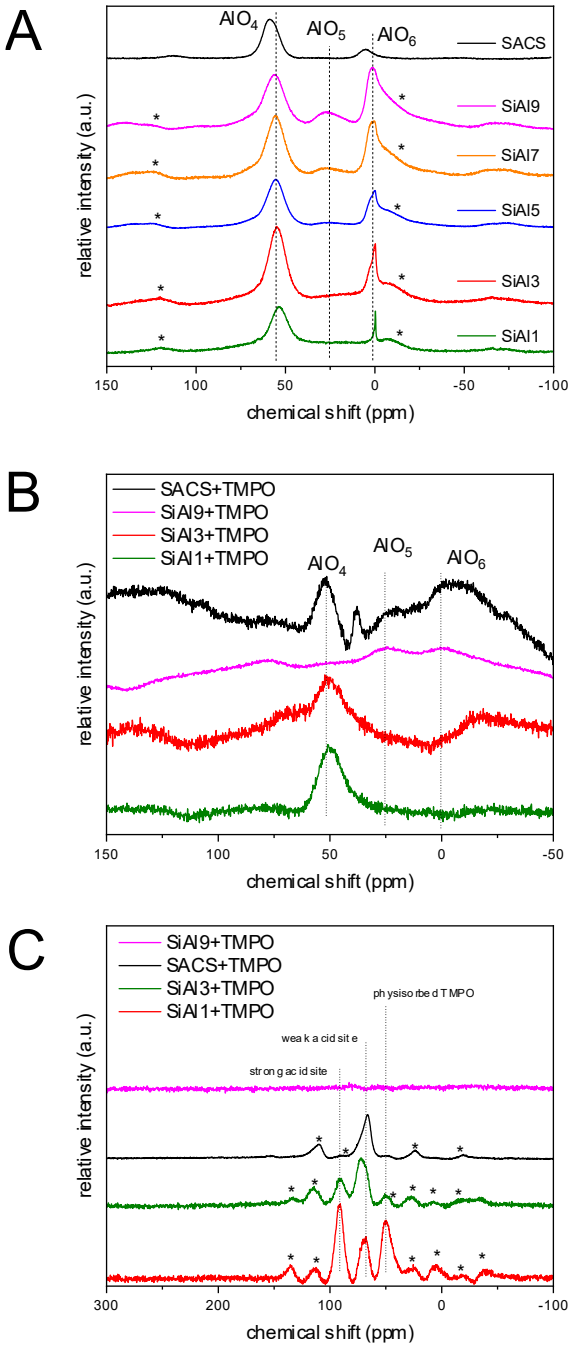

Figure 6: (A) ^{27}Al MAS NMR spectra of calcined aluminosilicates, (B) ^{27}Al MAS NMR spectra of aluminosilicates after exposure to TMPO, (C) ^{31}P MAS NMR spectra after adsorption of TMPO onto degassed aluminosilicates. Asterisks denote spinning side bands.

The samples acidity can be probed by adsorption of trimethyl phosphine oxide and analyzed by ^{31}P MAS NMR spectroscopy (Figure 6C). Besides **SiAl9** where no phosphorus signal was evident in the spectra (see discussion above), **SiAl1** and **SiAl3** showed three distinguished peaks with chemical shifts 47, 67, and 90 ppm (Figure 6C) suggesting the presence of acid sites with different strengths. While the signal at 47 ppm represents physisorbed TMPO,[86] signals shifted downfield, i.e. 67 and 90 ppm, are related to

chemisorbed TMPO. The former one could originate from the interaction of silanol groups on the surface with TMPO molecules,[32] while the latter are tentatively ascribed to strong acid sites. Interestingly, the discerned chemical shifts in AASG aluminosilicates are similar to TMPO adsorbed on zeolites. The signals at 67, 86 and 63 ppm were observed in H-ZSM-5 after TMPO adsorption and related to internal and external acid sites in H-ZSM-5 zeolites.[87] Signal at higher chemical shift (86 ppm) has been reported as a threshold for superacidity.[88] In comparison, commercial SACS exhibited signal at 67 ppm suggesting the presence of silanol groups but no signals at a higher chemical shift indicating the presence of only weak acid sites in SACS. In other words, aerosol-made aluminosilicate (with low Al loading) clearly exhibits much stronger acid sites as compared to the commercial benchmark obtained by coprecipitation (in agreement with IR spectroscopy combined with adsorption of pyridine, see below).

Pyridine (kinetic diameter = 0.54 nm) was used for acid site analysis by infrared spectroscopy (IR-py). First, the OH region of dehydrated samples prior to the adsorption of pyridine is depicted in Figure 7A (dark lines). Stretching vibration of isolated SiOH groups at 3742 cm^{-1} is visible in all samples degassed at 350 °C. After pyridine adsorption, absorption band for stretching vibration of SiOH groups (Figure 7A, light lines) decreased in intensity apparently due to pyridine chemisorption.[89] Only the samples with higher Al loading after the desorption of pyridine at 150 °C provided very similar intensity of stretching SiOH band as only degassed at 350 °C, suggesting limited amount of acidic OH groups interacting with pyridine.

Nevertheless, all aluminosilicates provided absorption bands confirming presence of acid sites, typically detected in the region between 1700 and 1350 cm^{-1}. Usually, both Brønsted and Lewis acid sites are found in amorphous aluminosilicates.[33,90,91] Here, in the case of samples with higher aluminum loadings (**SiAl5**, **SiAl7**, and **SiAl9**) the number of Brønsted acid sites is negligible and should be evaluated cautiously (Figure 7B). Lewis acidity was also very low for these samples, reaching up to 35 µmol g^{-1} for **SiAl7**. On the other hand, the total amount of acid sites (Brønsted and Lewis, Figure 7C, Figure 7D and Table 5) after desorption at 150 °C for **SiAl1** and **SiAl3** was more than doubled compared to **SiAl7**, namely 73 and 113 µmol g^{-1}, respectively (Figure S7).

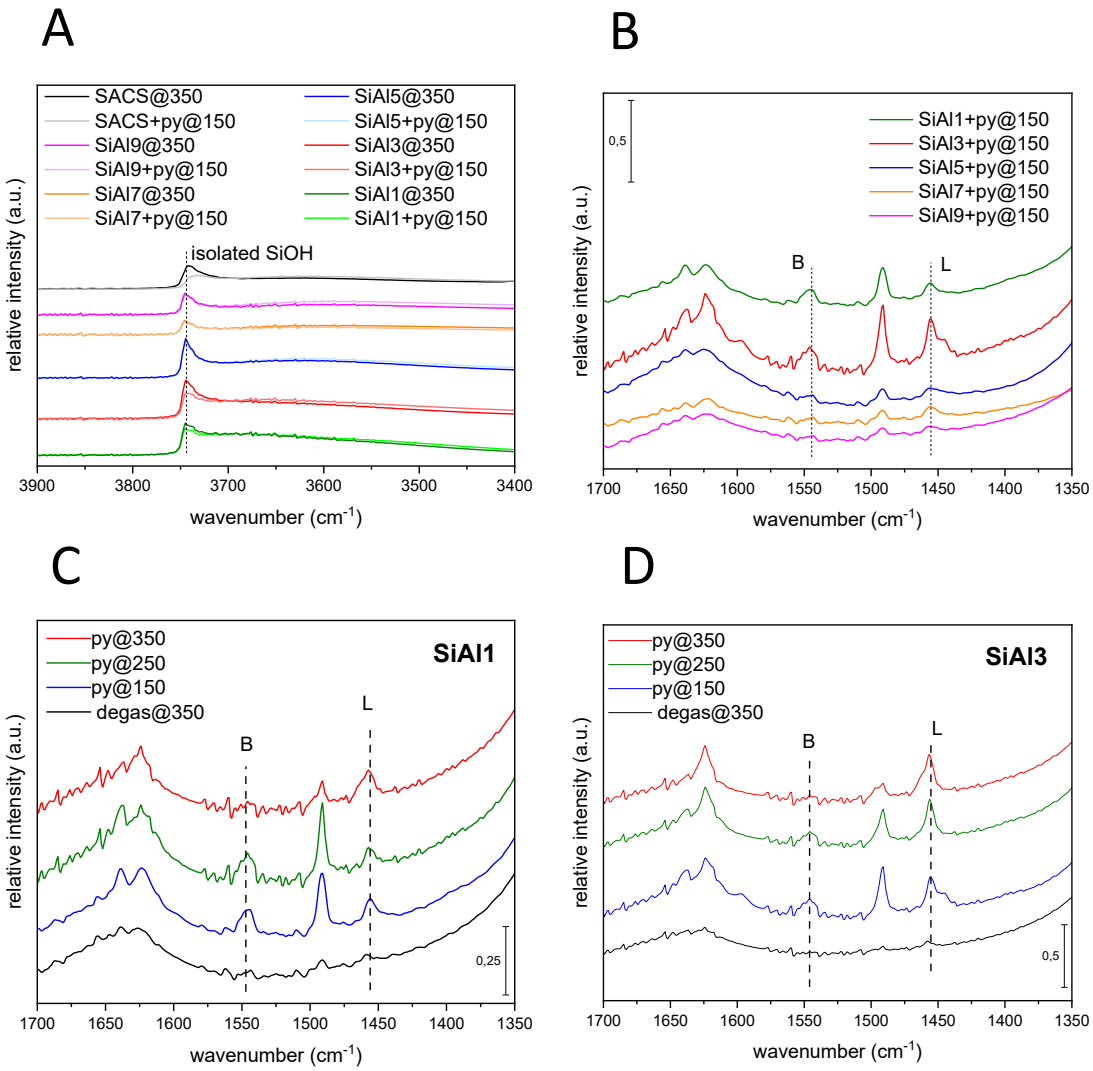

Figure 7: Infrared spectra of (A) OH region of degassed aluminosilicates at 350 °C (dark lines) and after desorption of pyridine at 150 °C (light lines), (B) SiAl5, SiAl7, and SiAl9 after desorption of pyridine at 150 °C, (C and D) SiAl1 and SiAl3 degassed at 350 °C and after desorption of pyridine at 150, 250, and 350 °C

The strength of acid sites was evaluated as the fraction of acid sites probed by pyridine and retained after desorption at 350 °C (Table 5). While **SiAl1** retained less than 50 % of its acid sites, indicating relatively mild acidity, other samples with higher aluminum loadings maintained over 60 %, demonstrating stronger acidity. The weakest acid sites were exhibited by SACS (only 33 % retained after pyridine desorption at 350 °C).[33] The similar character of acid sites was observed by TMPO analysis (similar pretreatment conditions) where signal at 67 ppm in ^{31}P MAS NMR spectra (Figure 6C) suggested the presence of weak acid sites (e.g., silanol groups).

Table 5: Nature, amount, strength of acid sites in aluminosilicates determined by IR-py

sample	B/L after desorption			Total acid sites after desorption (µmol g^{-1})			Acid sites after desorption (%)	
	150 °C	250 °C	350 °C	150 °C	250 °C	350 °C	250 °C	350 °C
SiAl1	1.3	1.6	0	73	67	36	91	49
SiAl3	0.64	0.63	0	113	88	72	78	64
SiAl5	0	0	0	21	13	16	62	74
SiAl7	0	0	0	35	34	30	96	85
SiAl9	0	0	0	17	16	12	98	71
SACS[33]	0.24	0.40	0.054	138	42	46	31	33

4.3 Catalytic activity in ethanol dehydration

Calcined silica and aluminosilicates were tested in the ethanol dehydration reaction, in a fixed bed flow reactor in the 205–310 °C range, with a WHSV = 1.1 h^{-1} (Figure 8 and Table S3). Undoped silica showed negligible conversion at 275 °C and 310 °C producing only traces of butadiene and diethyl ether. Aluminosilicate samples led to the production of two major products: ethylene and diethyl ether. While diethyl ether was produced at lower temperatures, ethylene was favored at higher temperatures. At the higher temperatures (mainly 275 and 310 °C), a small amount of butadiene was detected with all samples and with **SiAl3** and **SiAl5** propylene was detected as well. The carbon balance based on all compounds was always close to 100 %.

Ethanol conversion (Figure 8) was mediocre over samples with higher aluminum loadings, reaching up to 59 %, 43 %, and 56 % for **SiAl5**, **SiAl7**, **SiAl9** at 310 °C, respectively. Higher conversions were achieved by the commercial silica-alumina support converting 73 % ethanol at 275 °C. However, at the same temperature of 275 °C 88 % and 100 % conversions were reached over **SiAl1** and **SiAl3**, respectively. At the temperature of only 240 °C **SiAl1** and **SiAl3** already exhibited high conversion (65 % and 85 %, respectively).

Unlike the calcined **SiAl7** which was virtually inactive, **SiAl7-washed** performed very well converting ethanol out of 50 % and 100 % at 205 and 240 °C, respectively (Figure 8). This amplifies the power of aerosol spray-drying preparation.

Selectivity to ethylene (Figure S8) over benchmark SACS reached 38 % at 275 °C. Similar or lower selectivities were achieved by highly Al loaded samples. Imposingly, samples with low loadings (**SiAl1** and **SiAl3)** yielded ethylene with selectivity of 98 % at the same temperature. High selectivity was also observed with **SiAl3** at 240 °C, reaching 81 %. Remarkably, selectivity to ethylene was pronounced in the case of **SiAl7-washed** where selectivity to ethylene was kept to 88 and 100 % at 240 and 275 °C, respectively. A more appropriate[46] comparison of selectivity to ethylene at iso-conversion is presented in the “Stability” section (vide infra).

Among all tested catalysts, ethylene yield over SACS and the higher Al-loaded samples (**SiAl5**, **SiAl7**, and **SiAl9**) at 240 °C displayed ethylene yields below 11 % (Figure 8) while **SiAl1** reached 27 %. In comparison, **SiAl3** emerges as the most promising calcined catalyst, achieving a 70% yield at 240 °C. Besides,

SiAl7-washed stands out with an exceptional 88 % yield at 240 °C (Figure 8), showcasing its remarkable potential.

This result clearly demonstrates the superior performance of **SiAl3** and highlights **SiAl7-washed** as a breakthrough solution, underscoring the importance of template-washing strategies for preserving texture, acidity, and therefore catalytic activity.

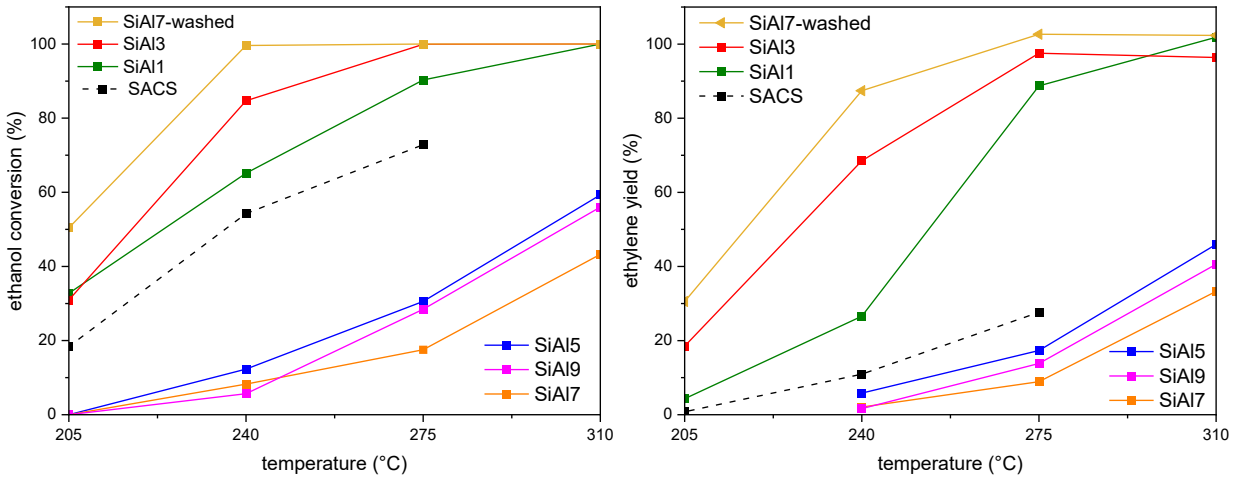

Figure 8: Ethanol conversion (left) and ethylene yield (right) over AASG prepared aluminosilicates and SACS during ethanol dehydration

These significant differences in catalytic activity can be attributed to both: (i) acid site amount, (ii) acid site strength (Table 5) determined by infrared spectroscopy combined with pyridine adsorption. First, **SiAl1** and **SiAl3** had at least twice the number of acid sites (73 and 113 µmol g^{-1}, respectively) reaching the highest ethylene yield compared to nearly catalytically inactive high Al-loading samples with minimal acidity (17 to 35 µmol g^{-1}). Second, while the relatively strong acid site of **SiAl3** (64 % acid sites remained after desorption at 350 °C) outcompeted all prepared catalysts, many weak acid sites (138 µmol g^{-1} retaining only 33 % at 350 °C) of commercial benchmark dropped behind with ethylene yield.

An apparent turnover frequency (TOF) was evaluated at 240 °C (Figure 9) considering the active sites as being the total number of acid sites retained after pyridine desorption at 150 °C (Table 5). TOF of commercial silica-alumina support SACS reached 94 h^{-1}. The efficiency of SACS acid sites was poor as the conversion was low and acid site concentration was high. Similar TOF values (56 and 81 h^{-1}) were reached by **SiAl7** and **SiAl9**, respectively. Higher TOF was reached by **SiAl5** (140 h^{-1}) and **SiAl3** (179 h^{-1}). Unequivocally, TOF for **SiAl1** reached the highest value, i.e. 492 mol ethanol converted per mol acid site per h, five times higher than commercial SACS and even two times higher than NHSG-prepared post-modified hybrid aluminosilicate catalysts under similar conditions (245 h^{-1}).[32]

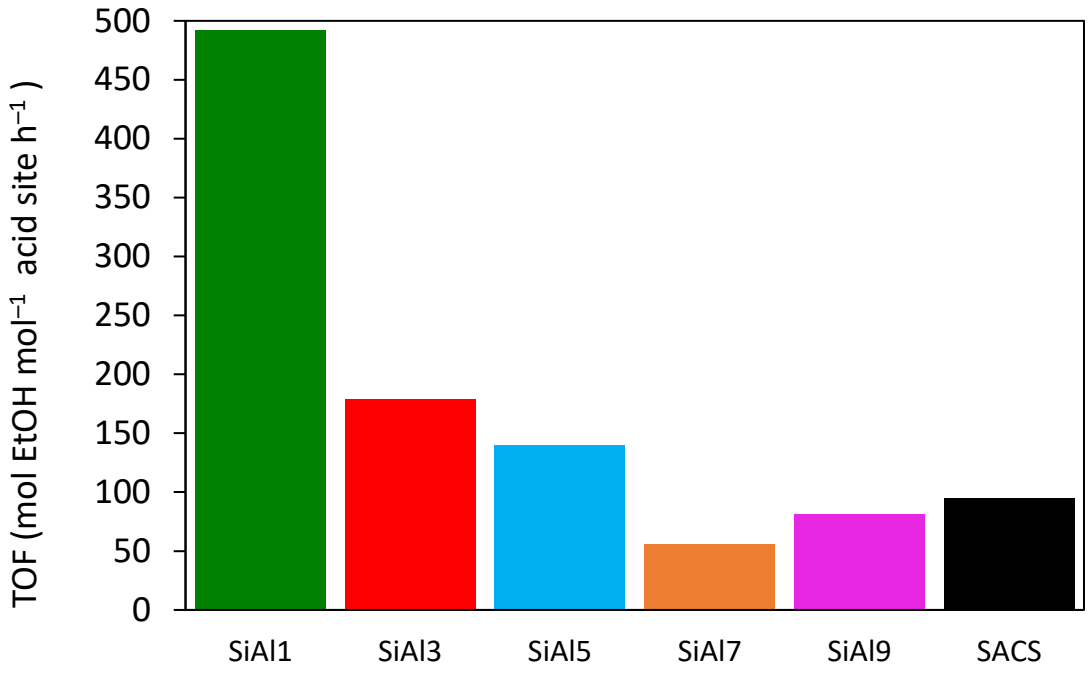

Figure 9: Turnover frequency evaluated at 240 °C for different aluminosilicate catalysts

4.4 Stability test and catalyst regeneration

The most active calcined catalysts (**SiAl1**, **SiAl3**, SACS) were selected for stability tests – 48 hours time-one-stream (TOS). It should be noted that the stability test herein was examined for a relatively long time compared to other studies.[31,33,35] Stability tests proceeded at 240 °C at iso-conversion of around 65 % (adjusting WHSV by changing the catalyst amount or the flow of ethanol mixture). At the onset of deactivation (similar conversions, Figure 10), the selectivity among samples can be evaluated (Figure 10). Ethylene selectivity over SACS reached 12 %. In contrast, the selectivity of AASG-prepared catalysts significantly outperformed the commercial SACS, achieving values at least 3.8 times higher — 56 % for **SiAl3** and 46 % for **SiAl1**. Interestingly, selectivity was stable during TOS for **SiAl1** and **SiAl3**, while it increased for SACS. Nevertheless, the selectivity to ethylene over SACS after 15 h TOS was still markedly lower (~26 %) in comparison to aluminosilicate samples prepared by AASG (**SiAl1** and **SiAl3**).

Evaluating catalytic performance, commercial SACS showed a decline in ethanol conversion from 65 % to 48 % after 15 hours. Practically the same deactivation in time (17 % after 15 hours) was followed by **SiAl3**. On the other hand, **SiAl1** was much more stable, revealing a drop in conversion by only 16 % after 48 hours (Figure 10). Overall, **SiAl3** and **SiAl1** produced very good ethylene yields over time (Figure S9).

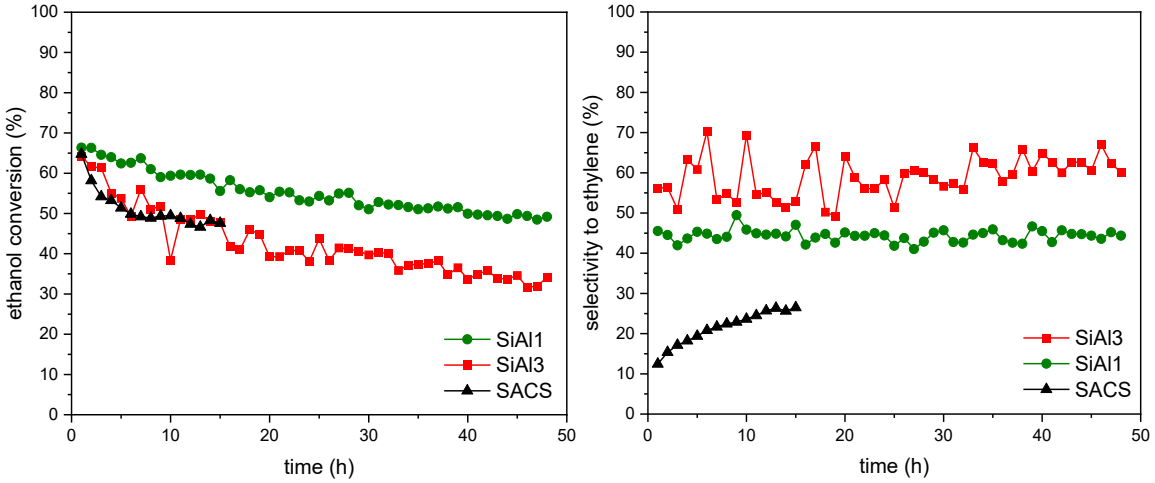

Figure 10: Stability test (ethanol conversion on the left, selectivity to ethylene on the right) over selected aluminosilicates

To better understand the deactivation phenomena, aluminosilicate catalysts prepared via aerosol-assisted sol-gel (AASG) were characterized after 48 hours on stream. The particles retained their spherical morphology and comparable size distribution according to SEM (Figure S10). The aluminum distribution remained homogeneous for both samples after catalysis according to STEM-EDS (Figure S11) excluding the high extent of aluminum oxide segregation. Moreover, ^{27}Al MAS NMR of hydrated samples after catalysis showed that the aluminum coordination was only slightly modified (possibly due to water adsorption during ethanol dehydration) but majority of aluminum remains four-coordinated similar to the fresh sample (Figure S12).

However, the color change of the AASG-prepared catalysts was visible (Figure S13). Whereas freshly calcined catalysts **SiAl1** and **SiAl3** were white after the synthesis, the color of spent **SiAl1** and spent **SiAl3** after 48 hours on stream darkened. The darker color of **SiAl3** suggests higher coke deposition on the surface of **SiAl3** catalysts. The presence of coke on the catalyst surface was confirmed by TG-DSC. While at the temperature below 200 °C, water and ethanol can be desorbed,[92] the mass loss at the higher temperature can be attributed to the carbon species combustion. The weight change of spent **SiAl3** from 200 °C up to 1000 °C was 10.27 %. On the other hand, mass change of spent **SiAl1** between the temperature range of 200 °C and 1000 °C was only 4.67 % (Figure S14, Table S4). The main weight loss in the case of spent **SiAl3** occurs between 400 °C and 650 °C, indicating one species of coke located in the same type of pores.

Pore clogging with carbonaceous species is also supported by nitrogen porosimetry (Figure S15, Table S5). While spent catalyst **SiAl3** completely lost its hysteresis loop, **SiAl1** still preserves the mesoporous structure. Thus, the changes in textural properties were much more pronounced in the case of **SiAl3**. Specific surface area dropped from 220 $m^2\ g^{-1}$ down to 50 $m^2\ g^{-1}$ (–77 %) whereas specific surface area of **SiAl1** slightly decreased – from 350 $m^2\ g^{-1}$ down to 300 $m^2\ g^{-1}$ (–14 %).

Finally, the coke nature was identified with ^{13}C CP MAS NMR performed on spent **SiAl3** catalyst (Figure S16). Besides residual reactants and products adsorbed on the catalyst's surface (ethanol and diethylether) with chemical shift of around 18 and 62 ppm, other signals appeared in the range of 21–50 ppm suggesting

the presence of alkanes[11] or oligomerized olefins.[93] No other carbonaceous species (aromatics, esters, alkenes, carboxylates) were detected.

The characterization of spent catalysts identified coking as the main source of deactivation. Moreover, it takes place to significantly higher extent in **SiAl3** in comparison to **SiAl1**. It can be suggested that this observation is related to the acid site strength. **SiAl3** contains a higher proportion of stronger acid sites (Table 5) and promotes coking to a higher extent. A similar conclusion has already been suggested when comparing mildly acidic amorphous aluminosilicates prepared by NHSG and zeolite HZSM-5.[33]

Importantly, strongly acidic zeolites are known to produce stable carbonaceous deposits based on aromatics (e.g., poly-substituted benzenes),[27] while alkanes and oligomerized olefins were observed in spent **SiAl3**. Thus, oxidative treatment of **SiAl3** after 48 hours on stream was performed at 550 °C to remove the carbonaceous deposit in the pores, rejuvenate the catalyst, and thus confirm the coke formation as the major contributor of deactivation. After 48 h on stream, ethanol conversion dropped down to 28 % and subsequent catalyst regeneration in oxygen flow restored the catalytic activity up to 48 % (Figure S17). Even though catalytic activity did not reach the original ethanol conversion (i.e., 65 %), it demonstrates successful regeneration of catalytic activity and suggests the carbon deposition as a major contributor of deactivation. The non-complete activity recovery could be assigned to the decrease of specific surface area after additional calcination treatment (observed for re-calcined fresh catalyst; Figure S18 and Table S6) or incomplete coke removal. Finally, a decrease of selectivity to ethylene after regeneration has been observed (Figure S17).

All in all, **SiAl1** is thought to possess an ideal acid site strength – not too weak as SACS, not too strong as **SiAl3**. The presence of medium acid strength to avoid coking has been already described.[33] A comparison of the catalysts synthesized in this study with state-of-the-art catalysts is valuable for evaluation. Comparing selectivity of purely inorganic spray-dried **SiAl3** with NHSG-prepared 16Si-1Al-Ac-T[33] at conversion of 85 % (at the same temperature of 240 °C), aerosol-made **SiAl3** exhibited 80 % selectivity towards ethylene compared to 55 % for aluminosilicate catalyst 16Si-1Al-Ac-T prepared by water-free sol-gel (noteworthy, **SiAl3** and 16Si-1Al-Ac-T contain very similar Al loading). However, considering NHSG-prepared hybrid aluminosilicates, the ethylene selectivity was significantly amplified by incorporation of methylsilyl groups.[34] This idea opens new possibilities for future research, particularly in exploring aerosol-assisted sol-gel synthesis to prepare hybrid materials and assess their catalytic performance in ethanol dehydration. Previous research has demonstrated that other one-pot prepared hybrid metallosilicates offer a superior alternative for purely inorganic materials in specific catalytic reactions,[94–96] not only in the terms of activity[32] but also long-term stability.[37]

5 Conclusion

We demonstrate that the aerosol-assisted sol-gel (AASG) method is a powerful, one-step strategy for producing aluminosilicate catalysts with excellent features for ethanol dehydration. One decisive feature of the aerosol synthesis is that the aluminum incorporation and distribution in the aluminosilicate materials was complete and homogeneous as confirmed by ICP-OES and STEM-EDS analyses with only 4-coordinated Al atoms determined by ^{27}Al MAS NMR after degassing and adsorption of TMPO. The

resulting aluminosilicates exhibit high surface areas, up to 350 $m^2 g^{-1}$, and a well-preserved porous structure at low Al loadings.

Crucially, the collapse of porosity observed at higher Al loadings (7–9 wt.%) during calcination is not an intrinsic limitation of AASG. Instead, we show that washing the template (Pluronic F-127) with ethanol, rather than removing it through calcination, successfully prevents pore collapse and maintains mesoporous material with enhanced catalytic activity. Ethanol washed **SiAl7-washed**, for instance, achieved an ethylene yield of 88 % at 240 °C, surpassing the performance of calcined **SiAl7** and **SiAl9**.

Impressively, aerosol-made catalysts with low loadings (**SiAl1**, **SiAl3**) exhibited at least three times higher ethylene yield in ethanol dehydration than a commercial aluminosilicate catalyst (SACS). While ethylene yield over SACS reached 28 % at 275 °C, ethylene yield over **SiAl1** and **SiAl3** was already 88 % and 100 % at 275 °C, respectively.

Moreover, **SiAl1** revealed 5-times higher TOF compared to commercial silica-alumina (492 and 94 mol EtOH per mol acid site per hour for **SiAl1** and SACS, respectively). This outstanding catalytic activity of **SiAl1** can be attributed to the well-dispersed acid sites over the silica matrix and much more efficient catalytic sites.

The time-on-stream stability over **SiAl1**, **SiAl3**, and SACS was tested. **SiAl3** and SACS deactivate fast – 30% loss in ethanol conversion. On the other hand, ethanol conversion was much more stable over **SiAl1** after 48 hours. These results indicate the importance of mildly acidic nature of **SiAl1** as determined by pyridine probe.

The proposed synthetic methodology benefits from the ease of industrial scale-up, enabling cost-effective catalyst production from basic and readily available precursors. Thus, it makes AASG highly competitive for industrial applications in catalyst production, with significant potential for improving the process for ethylene production.

6 Acknowledgment

The primary funding of this work was provided by the project Quantum materials for applications in sustainable technologies (QM4ST), CZ.02.01.01/00/22_008/0004572 by Program Johannes Amos Commenius, call Excellent Research. We acknowledge CF NMR of CIISB, Instruct-CZ Centre, supported by MEYS CR (LM2023042) and European Regional Development Fund-Project „Innovation of Czech Infrastructure for Integrative Structural Biology" (No. CZ.02.01.01/00/23_015/0008175). F.R.S.-FNRS is thanked for covering part of lab expenses of this research via CRD projects FNRS J.0044.20 and FNRS J.0042.25. The authors thank Dr. Zdenek Moravec for performing thermal analyses.

7 References

1 GlobalData, Production capacity of ethylene worldwide from 2018 to 2022 (in million metric tons), www.statista.com/statistics/1067372/global-ethylene-production-capacity.

2 M. W. M. van Goethem, S. Barendregt, J. Grievink, J. A. Moulijn and P. J. T. Verheijen, Ideal Chemical Conversion Concept for the Industrial Production of Ethene from Hydrocarbons, *Ind. Eng. Chem. Res.*, 2007, **46**, 4045–4062.

3 N. Rahimi and R. Karimzadeh, Catalytic cracking of hydrocarbons over modified ZSM-5 zeolites to produce light olefins: A review, *Appl. Catal. A Gen.*, 2011, **398**, 1–17.

4 A. M. Gaffney, J. W. Sims, V. J. Martin, N. V. Duprez, K. J. Louthan and K. L. Roberts, Evaluation and analysis of ethylene production using oxidative dehydrogenation, *Catal. Today*, 2021, **369**, 203–209.

5 G. Pampararo and D. P. Debecker, in *Reference Module in Chemistry, Molecular Sciences and Chemical Engineering*, Elsevier, 2024.

6 M. M. Mekonnen, T. L. Romanelli, C. Ray, A. Y. Hoekstra, A. J. Liska and C. M. U. Neale, Water, Energy, and Carbon Footprints of Bioethanol from the U.S. and Brazil, *Environ. Sci. Technol.*, 2018, **52**, 14508–14518.

7 X. Zhang, R. Wang, X. Yang and F. Zhang, Comparison of four catalysts in the catalytic dehydration of ethanol to ethylene, *Microporous Mesoporous Mater.*, 2008, **116**, 210–215.

8 Y. Schuurman, V. Ducarme, T. Chen, W. Li, C. Mirodatos and G. A. Martin, Low temperature oxidative dehydrogenation of ethane over catalysts based on group VIII metals, *Appl. Catal. A Gen.*, 1997, **163**, 227–235.

9 M. Marosz, A. Kowalczyk and L. Chmielarz, Modified vermiculites as effective catalysts for dehydration of methanol and ethanol, *Catal. Today*, 2020, **355**, 466–475.

10 M. E. Potter, E. B. McShane, N. L. Visser, J. D. Meeldijk, L. J. Allen, S. M. King, M. Carravetta, P. E. de Jongh, B. D. Vandegehuchte and R. Raja, Exploring the influence of mesoporosity in hard carbon-templated hierarchical SAPO-5 for ethanol dehydration, *RSC Appl. Interfaces*, 2024, **1**, 1360–1370.

11 C. P. Nash, A. Ramanathan, D. A. Ruddy, M. Behl, E. Gjersing, M. Griffin, H. Zhu, B. Subramaniam, J. A. Schaidle and J. E. Hensley, Mixed alcohol dehydration over Brønsted and Lewis acidic catalysts, *Appl. Catal. A Gen.*, 2016, **510**, 110–124.

12 T. K. Phung and G. Busca, Ethanol dehydration on silica-aluminas: Active sites and ethylene/diethyl ether selectivities, *Catal. Commun.*, 2015, **68**, 110–115.

13 P.-I. Dassie, R. Haddad, M. Lenez, A. Chaumonnot, M. Boualleg, P. Legriel, A. Styskalik, B. Haye, M. Selmane, D. P. Debecker, C. Sanchez, C. Chaneac and C. Boissiere, Coupling of solvent-free synthesis and reactive extrusion of alumina: an ecologically efficient integration for heterogenous catalyst synthesis, *Green Chem.*, 2023, **25**, 2800–2814.

14 T. K. Phung, A. Lagazzo, M. Á. Rivero Crespo, V. Sánchez Escribano and G. Busca, A study of commercial transition aluminas and of their catalytic activity in the dehydration of ethanol, *J. Catal.*, 2014, **311**, 102–113.

15 D. Yang, C. A. Gaggioli, D. Ray, M. Babucci, L. Gagliardi and B. C. Gates, Tuning Catalytic Sites on Zr 6 O 8 Metal–Organic Framework Nodes via Ligand and Defect Chemistry Probed with tert -Butyl Alcohol Dehydration to Isobutylene, *J. Am. Chem. Soc.*, 2020, **142**, 8044–8056.

16 X. Zhang, F.-Y. Cheng, H.-Z. Zhang, Z.-L. Xu, S.-M. Xue, X.-H. Ma and X.-R. Xu, In-situ synthetic modified metal-organic framework (MZIF-8) as an interlayer of the composite membranes for ethanol dehydration, *J. Memb. Sci.*, 2020, **601**, 117916.

17 C. Casas, R. Bringué, E. Ramírez, M. Iborra and J. Tejero, Liquid-phase dehydration of 1-octanol, 1-hexanol and 1-pentanol to linear symmetrical ethers over ion exchange resins, *Appl. Catal. A Gen.*, 2011, **396**, 129–139.

18 S. Andreoli, C. Oldani, V. Fiorini, S. Stagni, G. Fornasari and S. Albonetti, Superacid Aquivion® PFSA as an efficient catalyst for the gas phase dehydration of ethanol to ethylene in mild conditions, *Appl. Catal. A Gen.*, 2020, **597**, 117544.

19 M. Battisti, S. Andreoli, R. Bacile, C. Oldani, S. Ortelli, A. L. Costa, G. Fornasari and S. Albonetti, Aquivion® PFSA-based spray-freeze dried composite materials with SiO2 and TiO2 as hybrid catalysts for the gas phase dehydration of ethanol to ethylene in mild conditions., *Appl. Catal. A Gen.*, 2023, **654**, 119065.

20 J. M. Conesa, M. V. Morales, N. García-Bosch, I. R. Ramos and A. Guerrero-Ruiz, Graphite supported heteropolyacid as a regenerable catalyst in the dehydration of 1-butanol to butenes, *Catal. Today*, 2023, **420**, 114017.

21 W. Alharbi, E. Brown, E. F. Kozhevnikova and I. V. Kozhevnikov, Dehydration of ethanol over heteropoly acid catalysts in the gas phase, *J. Catal.*, 2014, **319**, 174–181.

22 L. Frattini, F. C. Jentoft, C. M. A. Parlett, V. D. B. C. Dasireddy, D. Jampaiah, H. Arandiyan, C. Len, A. F. Lee and K. Wilson, Ethanol Dehydration over Silica-Supported H 3 PW 12 O 40 and the Role of Water, *ACS Catal.*, 2025, **15**, 9430–9441.

23 J. Rorrer, S. Pindi, F. D. Toste and A. T. Bell, Effect of Alcohol Structure on the Kinetics of Etherification and Dehydration over Tungstated Zirconia, *ChemSusChem*, 2018, **11**, 3104–3111.

24 G. Chen, S. Li, F. Jiao and Q. Yuan, Catalytic dehydration of bioethanol to ethylene over TiO2/γ-Al2O3 catalysts in microchannel reactors, *Catal. Today*, 2007, **125**, 111–119.

25 T. K. Phung, L. Proietti Hernández and G. Busca, Conversion of ethanol over transition metal oxide catalysts: Effect of tungsta addition on catalytic behaviour of titania and zirconia, *Appl. Catal. A Gen.*, 2015, **489**, 180–187.

26 H. Ma, H. Gao, H. Jin, K. Li and D. Wen, High-pressure catalytic dehydration of ethanol to ethylene over microwave-synthesized nanocrystalline zeolite β, *Mater. Today Chem.*, 2025, **46**, 102775.

27 E. Catizzone, G. Ferrarelli, P. Bruno, G. Giordano and M. Migliori, Simultaneous catalytic dehydration of methanol and ethanol: How ZSM-5 acidity addresses conversion and products distribution, *Catal. Today*, 2024, **427**, 114436.

28 P. Pornsetmetakul, S. Klinyod, C. Rodaum, S. Salakhum, P. Iadrat, E. J. M. Hensen and C. Wattanakit, Fine-Tuning Texture of Highly Acidic HZSM-5 Zeolite for Efficient Ethanol Dehydration, *ChemCatChem*, , DOI:10.1002/cctc.202201387.

29 W. Zhao, J. Hua, Y. Cao, R. Yao and Y. Li, A rapid microwave-assisted solvothermal La3+ ion exchange of NaA zeolite membranes for enhanced performance of ethanol dehydration, *Microporous Mesoporous Mater.*, 2025, **392**, 113645.

30 J. S. Bates and R. Gounder, Clustering of alkanols confined in chabazite zeolites: Kinetic implications for dehydration of methanol-ethanol mixtures, *J. Catal.*, 2020, **390**, 178–183.

31 T. K. Phung, L. Proietti Hernández, A. Lagazzo and G. Busca, Dehydration of ethanol over zeolites, silica alumina and alumina: Lewis acidity, Brønsted acidity and confinement effects, *Appl. Catal. A Gen.*, 2015, **493**, 77–89.

32 L. Leonova, Z. Moravec, P. Sazama, J. Pastvova, L. Kobera, J. Brus and A. Styskalik, Hydrophobicity Boosts Catalytic Activity: The Tailoring of Aluminosilicates with Trimethylsilyl Groups**, *ChemCatChem*, , DOI:10.1002/cctc.202300449.

33 A. Styskalik, V. Vykoukal, L. Fusaro, C. Aprile and D. P. Debecker, Mildly acidic aluminosilicate catalysts for stable performance in ethanol dehydration, *Appl. Catal. B Environ.*, 2020, **271**, 118926.

34 A. Styskalik, I. Kordoghli, C. Poleunis, A. Delcorte, Z. Moravec, L. Simonikova, V. Kanicky, C. Aprile, L. Fusaro and D. P. Debecker, Hybrid mesoporous aluminosilicate catalysts obtained by non-hydrolytic sol–gel for ethanol dehydration, *J. Mater. Chem. A*, 2020, **8**, 23526–23542.

35 H. Xin, X. Li, Y. Fang, X. Yi, W. Hu, Y. Chu, F. Zhang, A. Zheng, H. Zhang and X. Li, Catalytic dehydration of ethanol over post-treated ZSM-5 zeolites, *J. Catal.*, 2014, **312**, 204–215.

36 A. Styskalik, I. Kordoghli, C. Poleunis, A. Delcorte, D. D. Dochain, Z. Moravec, J. Vida, T. Homola, C. Aprile, L. Fusaro, F. Devred and D. P. Debecker, Non-hydrolytic sol–gel route to a family of hybrid mesoporous aluminosilicate ethanol dehydration catalysts, *J. Mater. Sci.*, 2021, **56**, 14001–14018.

37 A. Styskalik, I. Kordoghli, C. Poleunis, A. Delcorte, C. Aprile, L. Fusaro and D. P. Debecker, Highly porous hybrid metallosilicate materials prepared by non-hydrolytic sol-gel: Hydrothermal stability and catalytic properties in ethanol dehydration, *Microporous Mesoporous Mater.*, 2020, **297**, 110028.

38 D. P. Debecker, C. Boissière, G. Laurent, S. Huet, P. Eliaers, C. Sanchez and R. Backov, First acidic macro-mesocellular aluminosilicate monolithic foams “SiAl(HIPE)” and their catalytic properties, *Chem. Commun.*, 2015, **51**, 14018–14021.

39 Q. Sheng, K. Ling, Z. Li and L. Zhao, Effect of steam treatment on catalytic performance of HZSM-5 catalyst for ethanol dehydration to ethylene, *Fuel Process. Technol.*, 2013, **110**, 73–78.

40 P. Iadrat, N. Horii, T. Atithep and C. Wattanakit, Effect of Pore Connectivity of Pore-Opened Hierarchical MOR Zeolites on Catalytic Behaviors and Coke Formation in Ethanol Dehydration, *ACS Appl. Mater. Interfaces*, 2021, **13**, 8294–8305.

41 A. T. Aguayo, A. G. Gayubo, A. Atutxa, M. Olazar and J. Bilbao, Catalyst Deactivation by Coke in the Transformation of Aqueous Ethanol into Hydrocarbons. Kinetic Modeling and Acidity Deterioration of the Catalyst, *Ind. Eng. Chem. Res.*, 2002, **41**, 4216–4224.

42 A. Święs, A. Kowalczyk, B. Gil and L. Chmielarz, Dehydration of methanol and ethanol over ferrierite originated layered zeolites – the role of acidity and porous structure, *RSC Adv.*, 2022, **12**, 9395–9403.

43 L. Chmielarz, A. Kowalczyk, M. Skoczek, M. Rutkowska, B. Gil, P. Natkański, M. Radko, M. Motak, R. Dębek and J. Ryczkowski, Porous clay heterostructures intercalated with multicomponent pillars as catalysts for dehydration of alcohols, *Appl. Clay Sci.*, 2018, **160**, 116–125.

44 Ł. Kuterasiński, U. Filek, M. Gackowski, M. Zimowska, M. Ruggiero-Mikołajczyk and P. J. Jodłowski, Sonochemically prepared hierarchical MFI-type zeolites as active catalysts for catalytic

ethanol dehydration, *Ultrason. Sonochem.*, 2021, **74**, 105581.

45 R. Le Van Mao, T. M. Nguyen and G. P. McLaughlin, The bioethanol-to-ethylene (B.E.T.E.) process, *Appl. Catal.*, 1989, **48**, 265–277.

46 F. Schüth, M. D. Ward and J. M. Buriak, Common Pitfalls of Catalysis Manuscripts Submitted to Chemistry of Materials, *Chem. Mater.*, 2018, **30**, 3599–3600.

47 A. Styskalik, D. Skoda, C. Barnes and J. Pinkas, The Power of Non-Hydrolytic Sol-Gel Chemistry: A Review, *Catalysts*, 2017, **7**, 168.

48 D. P. Debecker and P. H. Mutin, Non-hydrolytic sol–gel routes to heterogeneous catalysts, *Chem. Soc. Rev.*, 2012, **41**, 3624–3650.

49 D. P. Debecker, Innovative Sol-Gel Routes for the Bottom-Up Preparation of Heterogeneous Catalysts, *Chem. Rec.*, 2018, **18**, 662–675.

50 D. D. Dochain, A. Stýskalík and D. P. Debecker, Ag- and Cu-Promoted Mesoporous Ta-SiO2 Catalysts Prepared by Non-Hydrolytic Sol-Gel for the Conversion of Ethanol to Butadiene, *Catalysts*, 2019, **9**, 920.

51 D. D. Dochain, A. Van Den Daelen, A. Styskalik, V. Vykoukal and D. P. Debecker, Aerosol-assisted sol–gel synthesis of mesoporous Ag–Ta–SiO 2 catalysts for the direct upgrading of ethanol to butadiene, *RSC Sustain.*, 2023, **1**, 599–608.

52 D. P. Debecker, S. Le Bras, C. Boissière, A. Chaumonnot and C. Sanchez, Aerosol processing: a wind of innovation in the field of advanced heterogeneous catalysts, *Chem. Soc. Rev.*, 2018, **47**, 4112–4155.

53 S. Wintzheimer, L. Luthardt, K. L. A. Cao, I. Imaz, D. Maspoch, T. Ogi, A. Bück, D. P. Debecker, M. Faustini and K. Mandel, Multifunctional, Hybrid Materials Design via Spray-Drying: Much more than Just Drying, *Adv. Mater.*, , DOI:10.1002/adma.202306648.

54 S. Fiorilli, V. Cauda, L. Pontiroli, C. Vitale-Brovarone and B. Onida, Aerosol-assisted synthesis of mesoporous aluminosilicate microspheres: the effect of the aluminum precursor, *New J. Chem.*, 2016, **40**, 4420–4427.

55 S. Pega, C. Boissière, D. Grosso, T. Azaïs, A. Chaumonnot and C. Sanchez, Direct Aerosol Synthesis of Large-Pore Amorphous Mesostructured Aluminosilicates with Superior Acid-Catalytic Properties, *Angew. Chemie Int. Ed.*, 2009, **48**, 2784–2787.

56 S. Pega, C. Boissière, A. Chaumonnot and C. Sanchez, Tuning pore size and acidity of mesostructured aluminosilicates made by spray drying: design of new catalysts, *Stud. Surf. Sci. Catal.*, 2008, **174**, 471–476.

57 A. Vinu, V. Murugesan, W. Böhlmann and M. Hartmann, An Optimized Procedure for the Synthesis of AlSBA-15 with Large Pore Diameter and High Aluminum Content, *J. Phys. Chem. B*, 2004, **108**, 11496–11505.

58 D. P. Debecker, K. Bouchmella, C. Poleunis, P. Eloy, P. Bertrand, E. M. Gaigneaux and P. H. Mutin, Design of SiO 2 −Al 2 O 3 −MoO 3 Metathesis Catalysts by Nonhydrolytic Sol−Gel, *Chem. Mater.*, 2009, **21**, 2817–2824.

59 D. P. Debecker, M. Stoyanova, U. Rodemerck, F. Colbeau-Justin, C. Boissère, A. Chaumonnot, A.

Bonduelle and C. Sanchez, Aerosol route to nanostructured WO3-SiO2-Al2O3 metathesis catalysts: Toward higher propene yield, *Appl. Catal. A Gen.*, 2014, **470**, 458–466.

60 E. J. M. Hensen, D. G. Poduval, P. C. M. M. Magusin, A. E. Coumans and J. A. R. van Veen, Formation of acid sites in amorphous silica-alumina, *J. Catal.*, 2010, **269**, 201–218.

61 H. P. Jacobs, W. C. Elias, K. N. Heck, D. P. Dean, J. J. Dodson, W. Zhang, K. Hong, J. H. Arredondo, C. J. Breckner, L. Chen, S. G. Mueller, S. R. Alexander, J. T. Miller and M. S. Wong, Promotional Role of Acid Sites on Aluminosilicate-Supported PdAu for Vinyl Acetate Synthesis, *ACS Catal.*, 2024, **14**, 211–226.

62 S. M. Hosseini Asl, H. Javadian, M. Khavarpour, C. Belviso, M. Taghavi and M. Maghsudi, Porous adsorbents derived from coal fly ash as cost-effective and environmentally-friendly sources of aluminosilicate for sequestration of aqueous and gaseous pollutants: A review, *J. Clean. Prod.*, 2019, **208**, 1131–1147.

63 M. Stekrova, R. Zdenkova, M. Vesely, E. Vyskocilova and L. Cerveny, Immobilization of Methyltrioxorhenium on Mesoporous Aluminosilicate Materials, *Materials (Basel).*, 2014, **7**, 2650–2668.

64 D. Krajišnik, B. Čalija and J. Milić, in *Materials for Biomedical Engineering*, Elsevier, 2019, pp. 285–327.

65 N. Godard, A. Vivian, L. Fusaro, L. Cannavicci, C. Aprile and D. P. Debecker, High-Yield Synthesis of Ethyl Lactate with Mesoporous Tin Silicate Catalysts Prepared by an Aerosol-Assisted Sol-Gel Process, *ChemCatChem*, 2017, **9**, 2211–2218.

66 A. Vivian, L. Soumoy, L. Fusaro, P. Louette, A. Felten, S. Fiorilli, D. P. Debecker and C. Aprile, The high activity of mesoporous Ga-SiO2 catalysts in the upgrading of glycerol to solketal explained by in-depth characterization, *J. Catal.*, 2021, **400**, 83–92.

67 J. Poostforooshan, S. Belbekhouche, M. Shaban, V. Alphonse, D. Habert, N. Bousserrhine, J. Courty and A. P. Weber, Aerosol-Assisted Synthesis of Tailor-Made Hollow Mesoporous Silica Microspheres for Controlled Release of Antibacterial and Anticancer Agents, *ACS Appl. Mater. Interfaces*, 2020, **12**, 6885–6898.

68 Y.-K. Ma, S. Rigolet, L. Michelin, J.-L. Paillaud, S. Mintova, F. Khoerunnisa, T. J. Daou and E.-P. Ng, Facile and fast determination of Si/Al ratio of zeolites using FTIR spectroscopy technique, *Microporous Mesoporous Mater.*, 2021, **311**, 110683.

69 V. C. Farmer, Infrared spectroscopy in clay mineral studies, *Clay Miner.*, 1968, **7**, 373–387.

70 S. Maksasithorn, P. Praserthdam, K. Suriye and D. P. Debecker, Preparation of super-microporous WO3–SiO2 olefin metathesis catalysts by the aerosol-assisted sol–gel process, *Microporous Mesoporous Mater.*, 2015, **213**, 125–133.

71 G. Pampararo, G. Garbarino, P. Riani, V. Vykoukal, G. Busca and D. P. Debecker, Ethanol dehydrogenation to acetaldehyde with mesoporous Cu-SiO2 catalysts prepared by aerosol-assisted sol–gel, *Chem. Eng. J.*, 2023, **465**, 142715.

72 M. Toba, F. Mizukami, S. Niwa, T. Sano, K. Maeda and H. Shoji, Effect of preparation methods on properties of amorphous alumina/silicas, *J. Mater. Chem.*, 1994, **4**, 1131.

73 R. Mokaya and W. Jones, Direct Synthesis of Acidic Aluminosilicate Mesoporous Molecular Sieves, *MRS Proc.*, 1996, **431**, 83.

74 R. Dhanusha, P. M. Srinivasappa, S. C. Alla, M. Hemavathi, D. Prasad, N. K. Chaudhari and A. H. Jadhav, Efficient Selective Catalytic Fixation of CO 2 into Epoxide to Form Cyclic Carbonates Using Sodium Aluminate Engineered Gamma Alumina Catalyst, *Appl. Organomet. Chem.*, , DOI:10.1002/aoc.7429.

75 M. Jacquemin, M. J. Genet, E. M. Gaigneaux and D. P. Debecker, Calibration of the X-Ray Photoelectron Spectroscopy Binding Energy Scale for the Characterization of Heterogeneous Catalysts: Is Everything Really under Control?, *ChemPhysChem*, 2013, **14**, 3618–3626.

76 E. Lippmaa, M. Maegi, A. Samoson, M. Tarmak and G. Engelhardt, Investigation of the structure of zeolites by solid-state high-resolution silicon-29 NMR spectroscopy, *J. Am. Chem. Soc.*, 1981, **103**, 4992–4996.

77 M. May, M. Asomoza, T. Lopez and R. Gomez, Precursor Aluminum Effect in the Synthesis of Sol−Gel Si−Al Catalysts: FTIR and NMR Characterization, *Chem. Mater.*, 1997, **9**, 2395–2399.

78 A. Abraham, S.-H. Lee, C.-H. Shin, S. Bong Hong, R. Prins and J. A. van Bokhoven, Influence of framework silicon to aluminium ratio on aluminium coordination and distribution in zeolite Beta investigated by 27Al MAS and 27Al MQ MAS NMR, *Phys. Chem. Chem. Phys.*, 2004, **6**, 3031.

79 J. A. van Bokhoven, A. M. J. van der Eerden and D. C. Koningsberger, Three-Coordinate Aluminum in Zeolites Observed with In situ X-ray Absorption Near-Edge Spectroscopy at the Al K-Edge: Flexibility of Aluminum Coordinations in Zeolites, *J. Am. Chem. Soc.*, 2003, **125**, 7435–7442.

80 J. A. van Bokhoven, A. M. J. van der Eerden and D. C. Koningsberger, 2002, pp. 1885–1890.

81 E. J. M. Hensen, D. G. Poduval, V. Degirmenci, D. . J. M. Ligthart, W. Chen, F. Maugé, M. S. Rigutto and J. A. R. Van Veen, Acidity Characterization of Amorphous Silica–Alumina, *J. Phys. Chem. C*, 2012, **116**, 21416–21429.

82 L. Engelhardt, C. Raston, C. Whitaker and A. White, Crystal-Structure of Trimethylphosphine Oxide, *Aust. J. Chem.*, 1986, **39**, 2151.

83 J. Brus, L. Kobera, W. Schoefberger, M. Urbanová, P. Klein, P. Sazama, E. Tabor, S. Sklenak, A. V. Fishchuk and J. Dědeček, Structure of Framework Aluminum Lewis Sites and Perturbed Aluminum Atoms in Zeolites as Determined by 27 Al{ 1 H} REDOR (3Q) MAS NMR Spectroscopy and DFT/Molecular Mechanics, *Angew. Chemie Int. Ed.*, 2014, **54**, n/a-n/a.

84 M. Kejik, J. Brus, L. Jeremias, L. Simonikova, Z. Moravec, A. Styskalik, C. E. Barnes and J. Pinkas, Lewis Acidic Aluminosilicates: Synthesis, 27Al TQ/MAS NMR, and DFT-calculated 27Al NMR parameters.

85 J. Jiao, J. Kanellopoulos, W. Wang, S. S. Ray, H. Foerster, D. Freude and M. Hunger, Characterization of framework and extra-framework aluminum species in non-hydrated zeolites Y by 27Al spin-echo, high-speed MAS, and MQMAS NMR spectroscopy at B0= 9.4 to 17.6 T, *Phys. Chem. Chem. Phys.*, 2005, **7**, 3221.

86 H.-M. Kao, C.-Y. Yu and M.-C. Yeh, Detection of the inhomogeneity of Brønsted acidity in H-mordenite and H-β zeolites: a comparative NMR study using trimethylphosphine and trimethylphosphine oxide as P NMR probes, *Microporous Mesoporous Mater.*, 2002, **53**, 1–12.

87 Q. Zhao, W.-H. Chen, S.-J. Huang, Y.-C. Wu, H.-K. Lee and S.-B. Liu, Discernment and Quantification of Internal and External Acid Sites on Zeolites, *J. Phys. Chem. B*, 2002, **106**, 4462–4469.

88 A. Zheng, H. Zhang, X. Lu, S.-B. Liu and F. Deng, Theoretical Predictions of 31 P NMR Chemical Shift Threshold of Trimethylphosphine Oxide Absorbed on Solid Acid Catalysts, *J. Phys. Chem. B*, 2008, **112**, 4496–4505.

89 J. . Marques, I. Gener, P. Ayrault, J. . Bordado, J. . Lopes, F. Ramôa Ribeiro and M. Guisnet, Infrared spectroscopic study of the acid properties of dealuminated BEA zeolites, *Microporous Mesoporous Mater.*, 2003, **60**, 251–262.

90 T. Li, Z. Tao, L. Zhang and Y. Yang, Facile and cost-effective synthesis of acidity-enhanced amorphous silica-alumina for high-performance isomerization, *J. Solid State Chem.*, 2021, **300**, 122249.

91 K. Pyra, K. A. Tarach and K. Góra-Marek, Towards a greater olefin share in polypropylene cracking – Amorphous mesoporous aluminosilicate competes with zeolites, *Appl. Catal. B Environ.*, 2021, **297**, 120408.

92 A. Aloise, A. Marino, F. Dalena, G. Giorgianni, M. Migliori, L. Frusteri, C. Cannilla, G. Bonura, F. Frusteri and G. Giordano, Desilicated ZSM-5 zeolite: Catalytic performances assessment in methanol to DME dehydration, *Microporous Mesoporous Mater.*, 2020, **302**, 110198.

93 S. Zeng, J. Li, N. Wang, W. Zhang, Y. Wei, Z. Liu and S. Xu, Investigation of Ethanol Conversion on H-ZSM-5 Zeolite by in Situ Solid-State NMR, *Energy & Fuels*, 2021, **35**, 12319–12328.

94 A. Vivian, L. Fusaro, D. P. Debecker and C. Aprile, Mesoporous Methyl-Functionalized Sn-Silicates Generated by the Aerosol Process for the Sustainable Production of Ethyl Lactate, *ACS Sustain. Chem. Eng.*, 2018, **6**, 14095–14103.

95 L. E. Manangon-Perugachi, V. Smeets, A. Vivian, I. Kainthla, P. Eloy, C. Aprile, D. P. Debecker and E. M. Gaigneaux, Mesoporous Methyl-Functionalized Titanosilicate Produced by Aerosol Process for the Catalytic Epoxidation of Olefins, *Catalysts*, 2021, **11**, 196.

96 A. Vivian, L. Soumoy, L. Fusaro, S. Fiorilli, D. P. Debecker and C. Aprile, Surface-functionalized mesoporous gallosilicate catalysts for the efficient and sustainable upgrading of glycerol to solketal, *Green Chem.*, 2021, **23**, 354–366.